HHS Public Access

Author manuscript

J Alzheimers Dis. Author manuscript; available in PMC 2023 January 01.

Published in final edited form as:

J Alzheimers Dis. 2022 ; 85(3): 1077–1093. doi:10.3233/JAD-210629.

Assessing Sex-Specific Circadian, Metabolic, and Cognitive Phenotypes in the AβPP/PS1 and APP$^{NL-F/NL-F}$ Models of Alzheimer's Disease

Jesse Britz[a], **Emmanuel Ojo**[a], **Asmita Dhukhwa**[a], **Takashi Saito**[b], **Takaomi C. Saido**[c], **Erin R. Hascup**[a,d], **Kevin N. Hascup**[a,d,e], **Shelley A. Tischkau**[a,e,*]

[a]Department of Pharmacology, Southern Illinois University School of Medicine, Springfield, IL, USA

[b]Department of Neurocognitive Science, Institute of Brain Science, Nagoya City University Graduate School of Medical Sciences, Nagoya, Aichi, Japan

[c]Laboratory for Proteolytic Neuroscience, RIKEN Center for Brain Science, Wako, Saitama, Japan

[d]Department of Neurology, Dale and Deborah Smith Center for Alzheimer's Research and Treatment, Southern Illinois University School of Medicine, Springfield, IL, USA

[e]Department of Medical Microbiology, Immunology and Cell Biology, Southern Illinois University School of Medicine, Springfield, IL, USA

Abstract

Background: Circadian disruption has long been recognized as a symptom of Alzheimer's disease (AD); however, emerging data suggests that circadian dysfunction occurs early on in disease development, potentially preceding any noticeable cognitive deficits.

Objective: This study compares the onset of AD in male and female wild type (C57BL6/J), transgenic (AβPP/PS1), and knock-in (APP$^{NL-F/NL-F}$) AD mouse models from the period of plaque initiation (6 months) through 12 months.

Methods: Rhythmic daily activity patterns, glucose sensitivity, cognitive function (Morris water maze, MWM), and AD pathology (plaques formation) were assessed. A comparison was made across sexes.

Results: Sex-dependent hyperactivity in AβPP/PS1 mice was observed. In comparison to C57BL/6J animals, 6-month-old male AβPP/PS1 demonstrated nighttime hyperactivity, as did 12-month-old females. Female AβPP/PS1 animals performed significantly worse on a MWM task than AβPP/PS1 males at 12 months and trended toward increased plaque pathology. APP$^{NL-F/NL-F}$ 12-month-old males performed significantly worse on the MWM task compared to 12-month-old females. Significantly greater plaque pathology occurred in AβPP/PS1 animals

*Correspondence to: Shelley A. Tischkau, PhD, 801 N. Rutledge, Room 3289, Springfield, IL 62794-9629, USA. Tel.: +1 217 840 6724; stischkau@siumed.edu.

Authors' disclosures available online (https://www.j-alz.com/manuscript-disclosures/21-0629r2).

SUPPLEMENTARY MATERIAL

The supplementary material is available in the electronic version of this article: https://dx.doi.org/10.3233/JAD-210629.

as compared to $APP^{NL-F/NL-F}$ animals. Female AβPP/PS1 animals performed significantly worse than $APP^{NL-F/NL-F}$ animals in spatial learning and memory tasks, though this was reversed in males.

Conclusion: Taken together, this study provides novel insights into baseline sex differences, as well as characterizes baseline diurnal activity variations, in the AβPP/PS1 and $APP^{NL-F/NL-F}$ AD mouse models.

Keywords

Alzheimer's disease; amyloid-β; arginine vasopressin; circadian rhythm; cognition; glial fibrillary acidic protein; metabolism; vasoactive intestinal peptide

INTRODUCTION

As the average human life expectancy continues to increase, so does the prevalence of non-communicable disease. Currently, 1 in 10 people within the United States age 65 and older have Alzheimer's disease (AD) related dementia, with prevalence increasing with age. AD is characterized by the accumulation of amyloid-β (Aβ) plaques and neurofibrillary tau tangles, resulting in neurodegenerative processes that ultimately lead to progressive cognitive deficiencies [1, 2]. In addition to cognitive decline, circadian system disruption is a notable symptom in early AD development, often presenting as disrupted sleep/wake rhythms as well as increased restlessness and agitation toward dusk, termed "sundowning" [3, 4]. Circadian dysfunction may occur several years prior to dementia diagnosis, but until recently was characterized simply as a symptom of disease progression [5]. Current literature, however, suggests that circadian disruption may play a role in AD pathogenesis.

On the circuit level, the mammalian circadian system is organized in a hierarchical manner, with the suprachiasmatic nucleus (SCN) in the basal hypothalamus serving as the master oscillator, synchronizing peripheral tissue oscillators to regulate local and whole organism circadian physiology [6, 7]. The SCN receives glutamatergic input onto vasoactive intestinal peptide (VIP) containing neurons via the retinal hypothalamic tract to synchronize rhythms to the environmental 24-h light/dark cycle [8, 9]. These VIP-containing neurons provide interneuronal synchronization within the SCN to strengthen overt circadian output [9-11]. Within the SCN, arginine vasopressin (AVP)-containing neurons participate in generation of robust circadian rhythms and determination of circadian period, primarily via interneuronal coupling [12]. Of the many circadian outputs that are measurable, day/night variations in locomotor activity directly reflect diurnal biological rhythms in the SCN [13-15]. In addition to increased night-time activity and agitation, human AD patients may also experience neuronal cell loss in the SCN, specifically of AVP- and VIP-containing neurons, presenting a potential mechanism by which circadian dysfunction results from pathological progression [16-18]. However, the relationship between AD and circadian dysfunction is proving to be bidirectional, indicating that circadian disturbances via chronic jet-lag exposure or routine swing shifts in the workplace have the capacity to contribute to AD pathogenesis. Potential interactions include fluctuations in diurnal Aβ levels and glymphatic clearance, changes in the astrogliotic response to plaque development, disrupted cellular clocks and robust intracellular synchrony, oxidative stress, and neurodegeneration [19-22].

The AβPP/PS1 transgenic mouse line is one of the more commonly used animal models of AD. Initial plaque deposition is reported at around 6 months and progresses with aging. In addition, AβPP/PS1 mice do not form neurofibrillary tau tangles and present little to no neuronal cell loss, allowing for a focused approach to the role of Aβ in AD pathology [23, 24]. Recently, a knock-in model ($APP^{NLF/NLF}$) expressing a mutant human amyloid precursor protein (AβPP) gene under the endogenous mouse AβPP promoter has garnered attention [25]. The $APP^{NL\text{-}F/NL\text{-}F}$ expresses a humanized AβPP with both the Swedish and Iberian mutations, resulting in increased overall $Aβ_{40\text{-}42}$ production with preferential cleavage for $Aβ_{42}$ production, which is more prone to the oligomerization and plaque formation that is a hallmark in AD pathology [25, 26]. In addition, the $APP^{NL\text{-}F/NL\text{-}F}$ expresses AβPP with the appropriate cell type and temporal specificity, preventing the overproduction of other AβPP fragments that have the potential to be biologically active, thus further optimizing studies specific for examining Aβ. The $APP^{NL\text{-}F/NL\text{-}F}$ is reported to develop initial plaque deposition as early as 6 months, similar to AβPP/PS1 animals [25]. The goal of this study was to characterize differential diurnal activity patterns, metabolic, cognitive, and pathological changes as a result of AD development between these two animal models from the early stages of AD pathology to later stage disease development. In addition, both male and female animals were used for each respective AD model. As nearly two-thirds of people within the United States with AD are women, it is of high importance to examine potential sex differences in disease development that might occur in these two commonly used animal models.

METHODS

Animals

Protocols for animal use were approved by the Institutional Animal Care and Use Committee at Southern Illinois University School of Medicine. Eight-week-old male and female AβPP/PS1 (RRID:MMR_RC034832-JAX; Mo/HuAPP695swe/PS1-dE9) mice, $AβPP^{NL\text{-}F/NL\text{-}F}$ mice and controls (C57BL 6/J) (RRIF:IMSR_JAX:000664) were group housed and entrained to a control 12 : 12-h light: dark schedule with food and water *ad libitum.* Animals were aged under control conditions to 6- and 12-month endpoints. One month prior to the endpoint, animals underwent glucose tolerance test (GTT), then were individually housed and activity was monitored for 3 weeks measured using infrared-activity detectors (Minimitter, Bend, OR). Activity data were collected in 6-minute bins and analyzed using Clocklab software (Actimetrics, Evanston, IL). Following activity monitoring, mice underwent a Morris Water Maze (MWM) cognitive assessment. Following MWM, all animals were sacrificed at Zeitgeber time (ZT) 12, defined as the time of lights off, via cervical dislocation. Whole brain tissue was collected immediately following euthanasia and fixed in 4% paraformaldehyde for 24 h, then transferred to 20% sucrose for storage in 4°C.

Chemicals

All chemicals were prepared and stored according to manufacturer recommendations unless otherwise noted. Sodium chloride (Cat: 7647-14-5), Sucrose (Cat: 57-50-1), Sodium phosphate Dibasic, Anhydrous (Cat: 7558-79-4), Potassium chloride (Cat: 7447-40-7),

Dextrose (Cat: 50-99-7), and Bovine serum albumin (Fraction V) (Cat: 9048-46-8) were obtained from Thermo Fisher Scientific (Waltham, MA). Potassium phosphate (Cat: 7778-77-01) was obtained from Sigma-Aldrich Co. (St. Louis, MO). Triton X-100 (Cat: 807426) and Sodium borohydride (Cat: 102894) were obtained from MP Biomedicals (Santa Ana, CA). Rabbit polyclonal VIP antibody (Cat: 20077) and rabbit polyclonal AVP antibody (Cat: 20069) were obtained from Immunostar (Hudson, WI). Chicken polyclonal glial fibrillary acidic protein (GFAP) antibody (Cat: C-1373-50), Amylo-Glo®RTD™ (Cat: TR-300-AG) were obtained from Biosensis (Temecula, CA). Normal goat serum (Cat: S26-LITER) was obtained from Millipore (Burlington, MA). Goat anti-chicken IgY H&L (Alexa Fluor® 594) (Cat: ab150172). Goat anti-rabbit IgG H&L (Alexa Fluor® 594) (Cat: A11012) was obtained from Invitrogen.

Intraperitoneal (IP) glucose tolerance test (GTT)

Initial blood glucose measurements were taken at app. ZT 12 (time = 0) following a 15-h fast for GTT. Following the T = 0 measurement, a bolus of 20% glucose was injected IP at 2 g of glucose/kg body weight (b.w.). Blood glucose levels were then measured sequentially at 15, 30, 45, 60, and 120 min. Glucose measurements were taken from blood collected from the tail vein using a Contour Next EZ Glucometer (Parsippany, NJ).

Morris water maze

At either the 6- or 12-month randomly assigned endpoints, mice underwent cognitive assessment of spatial learning and memory recall using MWM. The paradigm consists of distinct visual clues placed around the room external to the maze borders by which the animals were trained to utilize in finding the location of a static, hidden platform (submerged 1 cm below an opaque water surface) across repeated trials. The MWM paradigm consists of 5 consecutive training days (3 90-s trials/day) with a minimum inter-trial-interval of 20 min. Starting quadrant was randomized per trial among 3 starting locations with no location repeated in a single day. Forty-eight hours post-training, mice underwent a 60-s probe trial from a singular starting location to determine memory-recall. The Annulus 40 was defined as a region 40 cm in diameter centered around the platform, which is different from the annulus zone used to assess searching strategies in annular analysis of MWM [27]. ANY-maze video tracking system (Stoelting Co., Wood Dale, IL; RRID:SCR 014289) was used to record animal navigation during the challenge and probe trials. The 3 trials per day were averaged for each animal in all analytical parameters. Mice were excluded from MWM analysis if $a > 75\%$ improvement in learning was not observed by the 5th training session due to implications that a lack of effective learning would have on the memory task during the probe trial. Number of animals excluded for each group can be found in Supplementary Table 1.

Immunofluorescence (IF) and analysis

20 μm SCN and hippocampal sections were taken using a cryostat (Model HM525 NX, ThermoFisher Scientific). Serial sections were taken every 4th section in the SCN and every 6th section in the hippocampus. SCN sections underwent IF using rabbit polyclonal VIP antibody and rabbit polyclonal AVP antibody. Sections were permeabilized in PBST (0.1 M PBS with 0.25% TritonX-100) followed by 3 × 10-min washes in sodium borohydride

in PBS (1 mg/ml) for antigen retrieval. To control for nonspecific binding, sections were washed 3 × 10 min with PBST and incubated in 10%, normal goat serum/1% BSA for 1 h. The sections were then incubated overnight in primary antibody in a humidity chamber at 4°C. The following day, sections were washed 4 × 10 min in PBST and incubated in secondary antibody Goat anti-rabbit IgG H&L (Alexa Fluor® 594) 1: 1000 for 2 h. The sections then underwent 1 final wash 4 × 10 min in PBST and were coverslipped using ProLong™ Gold antifade reagent with DAPI. Hippocampal sections underwent IF using Chicken polyclonal glial fibrillary acidic protein (GFAP) antibody 1 : 1000, Amylo-Glo®RTD™ 1 : 100. Prior to GFAP staining, slides were transferred to a 70% ethanol solution for 5 min followed by a 2-min rinse in PBS. A 1 : 100 dilution of 100X stock Amylo-Glo RTDTM was prepared fresh, and the sections were incubated for 10 min in the staining solution. Slides were then rinsed in 0.9% saline solution for 5 min without shaking and prepared for IHC by rinsing 3 × 2 min in PBS. Goat anti-chicken IgY H&L (Alexa Fluor® 594) 1 : 1000 was used as the secondary. Amylo-Glo/GFAP slides were coverslipped using ProLong Gold™ antifade reagent. Staining intensities for VIP, AVP, and GFAP were measured using National Institute of Health Image J Software 1.48 (RRID:SCR_003070). Similar areas +/−10% were measured within each region of the hippocampus for consistency. Images were captured on a Nikon Eclipse E-600 microscope equipped with an Olympus-750 video camera system, and a Dell Pentium III computer. Approximately 4 section per stain were obtained per animal. Staining density was obtained when background staining was subtracted from mean intensities. Amylo-Glo RTD™ stain was analyzed using the same equipment; however, measurements were calibrated in Image J software and recorded in mm^2.

Data analysis

Prism (GraphPad Software, Inc., La Jolla, CA; RRID:SCR_002798) software was used for statistical analyses. For locomotor activity analysis, fasting glucose, GTT AUC, and plaque number, a 2-way ANOVA was used. MWM Platform: corrected integrated path length (CIPL) and Platform: Latency to 1st entry measurements were analyzed using a 2-way ANOVA. Time spent in the annulus 40 and % time in the target quadrant for the probe trial, AVP and VIP mean fluorescence was analyzed using a one-way ANOVA. When the ANOVA indicated statistical significance, a Tukey's *post-hoc* test was used. Data are represented as mean ± SEM and statistical significance was defined as $p < 0.05$.

RESULTS

Sex-dependent hyperactivity and metabolic changes in relation to aging in AβPP/PS1 mice

Considering the bidirectional relationship proposed between AD and circadian system dysfunction, we sought to determine whether progressive AD pathology impacted diurnal locomotor activity levels in our AβPP/PS1 and $APP^{NL\text{-}F/NL\text{-}F}$ AD models. Male and female AβPP/PS1 mice, $APP^{NL\text{-}F/NL\text{-}F}$ mice, alongside C57BL/6J controls were aged to 6- and 12-month endpoints to assess the impact of progressive AD pathology from the onset of plaque pathology outward on daily rhythmic activity, metabolism, and cognition. In female mice, there was a significant main effect of animal group ($F_{5,184} = 4.574$, $p = 0.0006$), as well as lighting conditions ($F_{1,184} = 329.8$, $p < 0.0001$.) in home cage activity. There

was no interaction between animal group and lighting conditions ($F_{5,184}$ = 0.8 8 76, p = 0.4906.) In male mice, there was a significant main effect of animal group ($F_{5,142}$ = 2.563, p = 0.0297), as well as lighting conditions ($F_{1,142}$ = 329.8, p < 0.0001.) in home cage activity. There was no interaction between animal group and time of day ($F_{5,184}$ = 0.8584, p = 0.5108.) Lights off activity patterns were significantly higher than lights on activity patterns within a group among all ages, sexes, and genotype. Nighttime activity was not significantly dampened with age under 12 : 12-h lighting conditions in C57BL/6J mice. Home cage activity was unchanged in 12-month-old C57BL/6J females as compared to 6-month-old C57BL/6J females. The ratio of lights off/lights on activity in females was not significantly changed as a result of aging in C57BL/6J females. In male C57BL/6J mice, there was no change in activity levels or activity ratios from 6-12 months of age. Similarly, no significant changes in diurnal activity patterns were observed in AβPP/PS1 mice of either sex as a result of aging from 6–12 months. Alongside AβPP/PS1 animals, male and female $APP^{NL\text{-}F/NL\text{-}F}$ mice were aged to 6- and 12-month endpoints to assess the impact of progressive AD pathology on rhythmic daily activity patterns. In comparison to C57BL/6J mice, AβPP/PS1 males displayed significant nighttime hyperactivity at 6 months. Similar AβPP/PS1 hyperactivity was seen in females at 12 months as compared to C57BL/6J mice. In contrast, $AβP^{NL\text{-}F/NL\text{-}F}$ mice displayed comparatively similar activity levels to controls (Fig. 1A, B).

Aging is associated with impaired glucose metabolism and progressive metabolic dysfunction in both males and females [28, 29]. Additionally, comorbidity between AD and type-2 diabetes is highly prevalent, thus it was our goal to characterize changes in glucose metabolism, as well as sex differences in the impact of aging from 6–12 months on metabolic function in the AβPP/PS1 and $AβP^{NL\text{-}F/NL\text{-}F}$ AD models [30, 31]. In female mice, a significant main effect of genotype was observed in fasting glucose levels ($F_{2,90}$ = 5.885, p = 0.004) and GTT AUC measurements ($F_{2,90}$ = 4.025, p = 0.0212). In male mice, there is a significant main effect of both age ($F_{1,74}$ = 5.038, p = 0.0278) and genotype ($F_{2,74}$ = 3.167, p = 0.0479) on fasting glucose levels, however not on GTT AUC measurements. A significant interaction was observed between genotype and age in both female ($F_{2,90}$ = 3.447, p = 0.0361) and male ($F_{2,73}$ = 3.279, p = 0.0433 GTT AUC measurements). Fasting glucose levels as well as AUC measurements remained unaltered as a result of aging from 6–12 months in both male and female C57BL/6J and $APP^{NL\text{-}F/NL\text{-}F}$ mice. Similarly, fasting glucose or AUC measurements were not changed from 6–12 months in AβPP/PS1 females. Male AβPP/PS1 animals, however, presented higher fasting glucose measurements at 12 months as compared to 6 months (Fig. 1C-F). 12-month-old female AβPP/PS1 mice presented significantly higher fasting glucose levels as compared to age- and sex-matched C57BL/6J mice. Similarly, female AβPP/PS1 demonstrated higher AUC measurements during the GTT at 6 months as compared to age- and sex-matched C67BL/6J mice.

AD pathology progresses in a sex-dependent manner in AβPP/PS1 mice

MWM was used to assess spatial learning and memory recall on all mice (Fig. 2). During the 5-day training session, a significant main effect in platform: CIPL was observed from day 1 to day 5 ($F_{4,160}$ = 36.21, p < 0.0001), indicating that all groups were able to effectively

learn the location of the hidden platform. A significant main effect of animals group was also observed on platform: CIPL ($F_{3,160} = 9.783$, $p < 0.0001$). No interaction between animal group and trial day across the 5-day training period was observed in platform: CIPL measurements ($F_{12,160} = 0.761$, $p = 0.6896$). 12-month-old female AβPP/PS1 mice presented significantly higher platform: CIPL measurements as compared to 6-month-old AβPP/PS1 female mice on day 3. On day 1 and day 3 of the 5-day training period, 12-month-old females presented significantly higher CIPL measurements than 12-month-old males (Fig. 2A). On the remaining training days, a similar trend of females presenting higher CIPL than males at 12 months was apparent, though did not reach significance. Day 1 differences could potentially be attributed to differences in short term memory, as data for each day is averaged across 3 independent trials. No significant differences were observed in latency to 1st entry to the platform location across training days in AβPP/PS1 mice ($F_{3,160} = 2.553$, $p = 0.0574$), though a significant main effect of latency to 1st entry was observed, indicating all groups had learned the location of the hidden platform ($F_{4,160} = 24.02$, $p < 0.0001$) (Fig. 2B). No interaction between animal group and trial day across the 5-day training period was observed in latency to 1st platform entry measurements ($F_{12,160} = 0.9468$, $p = 0.5021$). No differences were found in the probe trial within a sex from 6–12 months, as measured by percent time spent in the target quadrant ($F_{3,32} = 0.2024$, $p = 0.8939$), time spent in the annulus 40 ($F_{3,32} = 0.2041$, $p = 0.8928$), and CIPL from the platform area ($F_{3,32} = 2.38$, $p = 0.0874$) (Fig. 2C-E). No significant difference was observed between sexes in 12-month-old C57BL/6J animals on the MWM task, indicating the differences observed here are a result of sex-dependent effects on learning and memory as a result of AD phenotype at the 12-month endpoint (Supplementary Figure 1).

Aβ plaque burden was analyzed via total plaque number in each subregion of the hippocampus (dentate gyrus (DG), CA1, CA3) (Fig. 3). A main effect of age ($F_{1,15} = 137.6$, $p < 0.0001$) and hippocampal subregion ($F_{2,15} = 18.67$, $p < 0.0001$) was observed in female AβPP/PS1 mice on hippocampal plaque number. A significant interaction was also observed between age and hippocampal subregion on hippocampal plaque number ($F_{2,15} = 10.34$, $p = 0.0015$). Similarly, a main effect of age ($F_{1,15} = 12.63$, $p = 0.0023$) and hippocampal subregion ($F_{2,15} = 4.989$, $p = 0.0189$) was observed in female AβPP/PS1 mice on hippocampal plaque number. Plaque number was significantly higher at the 12-month endpoint as compared to 6-month-old animals in both male and female AβPP/PS1 mice across hippocampal subregions (Fig. 3A-C).

A main effect of age ($F_{1,12} = 16.11$, $p = 0.0017$) was observed in female AβPP/PS1 mice on hippocampal GFAP expression. A main effect of age ($F_{1,12} = 17.93$, $p = 0.0012$) and hippocampal subregion ($F_{2,12} = 8.329$, $p = 0.0054$) was observed in female AβPP/PS1 mice. No interaction between age and hippocampal subregion was observed in female ($F_{2,12} = 3.621$, $p = 0.0588$) or male ($F_{2,12} = 0.2443$, $p = 0.787$) AβPP/PS1 mice. GFAP expression was significantly higher at 12 months in the DG as compared to 6 months in AβPP/PS1 females and significantly higher in DG and CA1 in 12-month-old males as compared to 6 months (Fig. 3D, F, G). Though not statistically significant, plaque pathology in females trended at higher levels than males at the 12-month endpoint (Supplementary Figure 2). Merged images illustrate the astrogliotic response around plaque regions that was present at plaque sites of all cohorts (Fig. 3E).

Comparative AD phenotype and diurnal activity patterns between an $APP^{NL-F/NL-F}$ knock-in model and the AβPP/PS1 transgenic line

In $APP^{NL-F/NL-F}$ mice, no significant differences were found from 6–12 months in male or female mice as measured by platform: CIPL and latency to 1st entry to the platform location during the 5-day training session. There was, however, a significant main effect of platform: CIPL ($F_{4,175} = 50.42$, $p < 0.0001$) and latency to 1st platform entry ($F_{4,180} = 16.96$, $p < 0.0001$), indicating all groups learned the location of the hidden platform. Memory recall was significantly dampened in 12-month-old $APP^{NL-F/NL-F}$ males as compared to 12-month-old females, as measured by percent time spent in the target quadrant ($F_{3,36} = 3.288$, $p = 0.0316$), though differences in time spent in the annulus 40 did not significantly differ during the probe trial (Fig. 4D, E). No significant differences were found in platform: CIPL during the probe trial (Fig. 4C). Similar learning curves, in addition to statistically similar CIPL values on day 5 of the training phase suggests a similar spatial learning capacity, making both groups directly comparable for the day 8 probe challenge. Differences observed in the percent time spent in the target quadrant during the probe trial suggests dampened memory recall in males as compared to females in the $APP^{NL-F/NL-F}$ AD model at 12 months.

Six-month-old male AD models performed similarly during the 5-day training phase (Fig. 5B, F). A significant main effect of genotype ($F_{2,190} = 7.673$, $p = 0.0006$) and trial day ($F_{4,190} = 54.72$, $p < 0.0001$) was observed in 6-month-old females, with no interaction between genotype and trial day on platform: CIPL measurements through the 5-day training period in 6-month-old females ($F_{8,190} = 0.8069$, $p = 0.5972$). Similarly, a significant main effect of genotype ($F_{2,210} = 12.86$, $p < 0.0001$) and trial day ($F_{4,210} = 16.23$, $p < 0.0001$) was observed in 6-month-old females, with no interaction between genotype and trial day on latency to 1st entry to the platform location through the 5-day training period in 6-month-old females ($F_{8,210} = 0.2791$, $p = 0.9723$). A *post-hoc* analysis revealed that in 6-month-old females, $APP^{NL-F/NL-F}$ mice presented a significantly higher platform: CIPL value on day 1 as compared to C57BL/6J mice, and AβPP/PS1 mice presented an increased latency to 1st platform entry on day 1 and day 5 as compared to C57BL/6J mice (Fig. 5A, E). Total time spent in the annulus 40 and percent time spent in the target quadrant during the probe trial was not significantly different between genotypes in either sex or endpoint (Fig. 5C, D, G, H).

A significant main effect of genotype ($F_{2,190} = 7.673$, $p = 0.0006$) and trial day ($F_{4,190} = 54.72$, $p < 0.0001$) was observed in 12-month-old females, with no interaction between genotype and trial day on platform: CIPL measurements through the 5-day training period in 6-month-old females ($F_{8,190} = 0.8069$, $p = 0.5972$). Similarly, a significant main effect of genotype ($F_{2,165} = 8.612$, $p = 0.0003$) and trial day ($F_{4,165} = 20.86$, $p < 0.0001$) was observed in 12-month-old females, with no interaction between genotype and trial day on latency to 1st entry to the platform location through the 5-day training period in 6-month-old females ($F_{8,165} = 0.7166$, $p = 0.6767$). In 12-month-old females, AβPP/PS1 animals showed significantly higher platform: CIPL and latency to 1st platform entry values in MWM on day 3 and 5 on the training session over C57BL/6J controls, and significantly above $APP^{NL-F/NL-F}$ mice on day 3, suggesting significantly delayed spatial learning in AβPP/PS1 females at 12 months that was not present in $APP^{NL-F/NL-F}$ mice (Fig. 6A, E).

Male AβPP/PS1 mice performed similarly to C57BL/6J animals at 12 months, suggesting differential rates of cognitive decline between AβPP/PS1 males and females (Fig. 6B, F). A significant main effect of genotype ($F_{2,135} = 6.829$, $p = 0.0015$) and trial day ($F_{4,135} = 4.593$, $p = 0.0017$) was observed in 12-month-old females, with no interaction between genotype and trial day on latency to 1st entry to the platform location through the 5-day training period in 6-month-old females ($F_{8,135} = 1.38$, $p = 0.2108$). In 12-month-old males, $APP^{NL\text{-}F/NL\text{-}F}$ mice presented an increased latency to 1st platform entry on day 5 over AβPP/PS1 mice. No significant differences in time spent in the target quadrant and annulus 40 during the probe trial were observed (Fig. 6D, F, H). No significant differences were observed in platform: CIPL across the 5-day training phase between either AD model and C57BL/6J controls in 12-month-old males (Fig. 6B).

Similar to the AβPP/PS1 animals, a significant main effect of age ($F_{1,18} = 12.54$, $p = 0.0023$) and hippocampal subregion ($F_{2,18} = 4.629$, $p = 0.0239$) was observed in female $APP^{NL\text{-}F/NL\text{-}F}$ mice on hippocampal plaque number, with no significant interaction between age and hippocampal subregion ($F_{2,18} = 2.743$, $p = 0.0913$). Increased plaque burden in the $APP^{NL\text{-}F/NL\text{-}F}$ mice from 6 to 12 months was significant in females, but not males. It should, however, be noted that at 6 months, hippocampal plaque burden was minimal in the $APP^{NL\text{-}F/NL\text{-}F}$ AD model (Fig. 7A-C). In 12-month-old $APP^{NL\text{-}F/NL\text{-}F}$ males, there was a significant main effect of age on GFAP expression in the hippocampus ($F_{1,12} = 12.26$, $p = 0.0044$). 12-month-old male GFAP expression was significantly higher in the CA1 as compared to 6-month-old males. No significant differences were found in GFAP expression from 6–12 months in $APP^{NL\text{-}F/NL\text{-}F}$ females (Fig. 7D-F). Sex- and age-matched AβPP/PS1 animals presented significantly more plaque burden than $APP^{NL\text{-}F/NL\text{-}F}$ animals, indicating differential rates of AD pathological progression between these two models (Fig. 8A-F). In 6-month-old females, there was a significant main effect of genotype ($F_{1,18} = 13.52$, $p = 0.0017$) and hippocampal subregion ($F_{2,18} = 3.990$, $p = 0.0368$) on hippocampal amyloid plaque number, with no significant interaction between genotype and hippocampal subregion ($F_{2,18} = 3.107$, $p = 0.0693$). In 6-month-old males, there was a significant main effect of genotype ($F_{1,18} = 4.799$, $p = 0.0419$) on hippocampal amyloid plaque burden. In 12-month-old females, there was a significant main effect of genotype ($F_{1,15} = 193.7$, $p < 0.0001$) and hippocampal subregion ($F_{2,15} = 19.73$, $p < 0.0001$) on hippocampal amyloid plaque number, with a significant interaction between genotype and hippocampal subregion ($F_{2,12} = 14.53$, $p = 0.0003$). In 12-month-old males, there was a significant main effect of genotype ($F_{1,18} = 20.42$, $p = 0.0003$) and hippocampal subregion ($F_{2,18} = 3.875$, $p = 0.0398$) on hippocampal amyloid plaque number, with no significant interaction between genotype and hippocampal subregion ($F_{2,18} = 3.138$, $p = 0.0678$).

AVP and VIP expression in the SCN were measured via immunofluorescence in 6- and 12-month-old AβPP/PS1 mice of both sexes to determine if any circadian effects seen in our AD models were a result of circadian relevant neuropeptide loss. No significant differences were found as a result of AD progression in expression of either neuropeptide in comparison to C57BL/6J controls in either females (Fig. 9A-D) or males (Fig. 9E-H) by the 12-month time point. Similarly, there were no sex differences in AVP or VIP expression in either AD model at either the 6 or 12-month endpoints.

DISCUSSION

Increased hippocampal plaque burden in 12-month-old female AβPP/PS1 animals over 12-month-old males approached significance, correlating with previous studies in the cerebellum that indicated a 5–10 fold increase in free $A\beta_{42}$ and $A\beta_{40}$ as well as plaque deposition, though this sex difference was not present in cortex [32]. Independent of sex, there was significantly higher plaque deposition at 12 months as compared to 6 months, though did not reach significance in all hippocampal subregions. Age-related progression of amyloid deposition in AβPP/PS1 mice followed a similar pattern to previous studies whereby accumulation was first observed in the CA1 followed by DG and finally the CA3 [33]. Significant differences in plaque pathology were at times observed in some subregions of the hippocampus and not others. In the case of comparisons inclusive of $APP^{NL\text{-}F/NL\text{-}F}$, there was very little plaque pathology, even at the 12-month endpoint. In many circumstances, plaques existed clustered around a single point, presenting values under 5 for a whole subregion. If there was no such cluster, the value was often zero for a particular region in a particular sample. This created enhanced variability that could account for the lack of statistical significance in one subregion over another. There is very little data regarding the specific initiation of plaque pathology in one hippocampal subregion over another, particularly in the mouse models used for this study. Additionally, it is unclear if there are differences between strains in the spatial and temporal progression of plaque pathology throughout brain regions, and especially specific hippocampal subregions. Spatial and temporal progression of amyloid plaques in AD in humans observed plaque deposition in early Braak stages in the CA1, only presenting in the CA3 in latter stages [34]. This could explain why significance is often found in CA1 and DG, whereas the CA3 presents lesser plaque pathology, and thus may not change much from the age of plaque initiation by the endpoints used in this study.

A general increase in hippocampal reactive astrocytes, as measured via GFAP expression, was observed in AβPP/PS1 mice similar to previous studies [31]. The role of reactive astrocytes in AD pathology remains heavily debated. Astrocyte reactivity is heavily correlated with progressive plaque formation in AD, and it has been hypothesized that reactive astrocytes potentially contribute to plaque formation via upregulation of β-secretase, promoting cleavage of AβPP and amyloid formation [35]. Evidence also exists suggesting that astrocyte reactivity can impact synaptic function and enhance excitotoxicity through a downregulation of GLT-1 and glutamine synthetase [36]. This may partially account for the elevated hippocampal glutamate levels observed in AβPP/PS1 mice [33, 37]. Conversely, analysis of postmortem brain has shown that reactive astrocytes absorb Aβ [38, 39]. This suggests a mechanism by which astrocytes participate in Aβ clearance and mitigate plaque formation, either via secretion of Aβ degrading enzymes or potential phagocytosis. Katsouri et al. demonstrated that ablation of reactive astrocytes in the AβPP23/GFAP-TK mouse model of AD exacerbated disease pathology as shown by increased plaque pathology, cognitive deficiencies, and enhanced neuroinflammation [40]. Astrocytes also have an intricate relationship with the circadian system. Astrocytes are known to present daily rhythms, and rhythmic activity of astrocytes within the SCN has been shown to impact behavioral rhythmic output as shown via specific astrocytic deletion of the clock gene

Bmal1 or the CK1*ε tau* mutation, both of which lengthen the circadian period in clock gene expression and locomotor activity by targeting the cellular core clock machinery [41]. YKL-40, an astrocytic protein that increases with age and AD development, and has an inverse correlation with astrocytic phagocytosis of Aβ, is circadian-regulated [42]. Astrocytes present circadian patterns of proximity to synapses and dendritic branching, impacting hippocampal dependent learning and synaptic plasticity, presenting further possible implications of circadian disturbances in AD progression [43].

Aging has been associated with a multitude of circadian changes, including sleep fragmentation, dysynchrony between central and peripheral oscillators, altered light sensitivity and ability to entrain to shifting light cues, and a decline in amplitude and robustness of overt behavioral rhythms such as locomotor activity [44-46]. AVP- and VIP-containing neurons in the SCN are subject to neurodegeneration in later stage AD, thus it was important to determine whether changes in locomotor activity during the active period might be due to a change in expression of these peptides [16-18]. VIP neurons in the core of the SCN are directly responsive to light cues, and *in vivo* silencing of these neurons dampens reentrainment patterns to resetting cues via changes in rhythmic light exposure [47, 48]. In the 3xTg mouse model of AD, which develops both Aβ and tau pathology, a decrease in both AVP and VIP expression was found at 11 months, prompting the question of at what point through disease development this initiates, and if specific neuropeptide loss occurs across animal models of AD [49]. AVP neurons in the SCN shell are responsible for interneuronal synchronization between independently self-oscillating neurons, driving robust rhythmic neuronal firing patterns [12]. We did not see any significant differences in either of these neuropeptides at 6 or 12 months between our AD models and C57BL/6J controls of either sex. Additionally, we did not find any significant changes in AVP or VIP from 6–12 months in either of the AD models used in this study. It would be interesting to determine if chronic circadian disruption throughout disease development could serve as a second insult to exacerbate AVP and VIP loss in the SCN.

Interstitial fluid (ISF) free Aβ levels have a diurnal rhythmicity. Chronic circadian disruption could potentially impact rhythmic fluctuations in ISF Aβ levels and amyloid clearance [19, 20]. Additionally, multiple genes involved in AβPP processing are circadian rhythmic [50]. Similarly, forced sleep disturbances in an AβPP/PS1 AD mouse model increased plaque burden, while increased sleep pressure via an orexin receptor antagonist reduced plaque formation [19, 21]. Though there is not an abundance of research describing the potential role of circadian rhythms as a contributing factor to AD development, future studies manipulating the circadian system throughout AD development could be beneficial in elucidating potential mechanisms.

The onset of cognitive impairment in AβPP/PS1 animals is reported to occur around 12 months, thus the lack of significance in males from 6–12 months in MWM performance was not surprising [51]. Females had significantly higher platform CIPL values during the 5-day training phase as compared to males at 12 months of age, and there were significantly higher CIPL values in 12-month-old females as compared to 6-month-old females on day 3. Similarly, trending data indicated an increased time spent in the annulus 40 in the probe trial in 12-month-old males as compared to females, indicating dampened spatial memory

in females. The significant increases in Day 3 Platform: CIPL and Latency to 1st platform entry in C57BL/6J animals above both AD models was surprising, though at 6 months of age, highly significant learning and memory deficits were not expected in either AD model. Additionally, all groups were statistically similar by day 5 of the 5-day training phase, indicating that all groups had effectively learned the location of the platform.

The correlation between aging and the development of metabolic syndrome has been well established; however, sex dependent differences in how aging impacts glucose are still being studied and remain highly significant for the development of sex-dependent therapeutic strategies [28]. Though statistically nonsignificant, the trending drop in glucose tolerance in females from 6–12 months is consistent with the number of biological changes that occur in females between the 6- and 12-month time points impacting glucose homeostasis, specifically the sharp drop that occurs in estrogen levels upon reproductive senescence at approximately 9–12 months in mice [52-54]. Studies suggest a potential link for altered insulin signaling and AD development, including accelerated Aβ accumulation, elevated hippocampal glutamate, and increased neuroinflammation [31, 55]. While our results did not elucidate any effect of progressive AD pathology in female AβPP/PS1 animals from 6–12 months, male animals did present higher fasting glucose levels at 12 months as compared to 6 months, contrasting the lack of an effect of aging in male C57BL/6J animals.

Using both the AβPP/PS1 and the $APP^{NL\text{-}F/NL\text{-}F}$ AD models provided useful insight as to how these models compare in terms of AD pathology, cognitive decline, and circadian function. Additionally, the use of both male and female animals presented novel findings regarding sex differences in these models. The use of the $APP^{NL\text{-}F/NL\text{-}F}$ knock-in models could potentially serve to elucidate specific effects of Aβ going forward, as this model does not rely on the tremendous overexpression and cleavage of AβPP, leading to other potentially physiologically active AβPP fragments. While the $APP^{NL\text{-}F/NL\text{-}F}$ presented similar plaque pathology as the AβPP model at 6 months, there were clear differential rates of progression between the two models up to the 12-month endpoint. Of particular interest were the differential sex differences between these two models in the memory recall portion of the MWM cognitive assessment. While some sex differences have been reported in the AβPP/PS1 model regarding Aβ production, the $APP^{NL\text{-}F/NL\text{-}F}$ model is relatively new, and significant sex differences in cognitive performance on the MWM task have not been previously reported [25, 32]. Considering the slow rate of plaque development in the $APP^{NL\text{-}F/NL\text{-}F}$ model, it would be worth assessing potential sex differences in plaque pathology at a later age. Incorporating a characterization of sex differences in these models as well as a side-byside comparison of pathological progression and AD phenotype provides useful data for model choice in future studies as well as dissecting the role of sex in AD development.

CONCLUSION

The current study indicates sex differences in how aging and AD progression impacts diurnal locomotor activity levels as well as glucose homeostasis and cognitive decline. Sex differences were observed in the AD phenotype, specifically cognitive performance on the MWM task in AβPP/PS1 mice, particularly at the 12-month time point, which

indicates differential rates of AD progression in the AD mouse. In side-by-side comparison of the AβPP/PS1 transgenic and the $APP^{NL-F/NL-F}$ knock-in models, AD pathology, as measured by plaque burden, progressed at a much higher rate in the transgenic line from plaque initiation at around 6 months in both models. In 12-month-old female animals, the AβPP/PS1 transgenic line performed worse on the MWM cognitive task in compared to the $APP^{NL-F/NL-F}$ mice. Future studies aim to look at how chronic circadian disruption throughout AD progression might impact the rate or severity of the AD development in these models.

Supplementary Material

Refer to Web version on PubMed Central for supplementary material.

ACKNOWLEDGMENTS

The research reported in this publication was supported by SIU Medicine and the SIU Medicine Team Development Grant. A special thank you also to Stacey Krager for weekly technical support and lab maintenance. NIH grants R01AG057767 and R01AG061937.

REFERENCES

[1]. Jack CR Jr., Knopman DS, Jagust WJ, Petersen RC, Weiner MW, Aisen PS, Shaw LM, Vemuri P, Wiste HJ, Weigand SD, Lesnick TG, Pankratz VS, Donohue MC, Trojanowski JQ (2013) Tracking pathophysiological processes in Alzheimer's disease: An updated hypothetical model of dynamic biomarkers. Lancet Neurol 12, 207–216. [PubMed: 23332364]

[2]. Selkoe DJ (2004) Cell biology of protein misfolding: The examples of Alzheimer's and Parkinson's diseases. Nat Cell Biol 6, 1054–1061. [PubMed: 15516999]

[3]. Peter-Derex L, Yammine P, Bastuji H, Croisile B (2015) Sleep and Alzheimer's disease. Sleep Med Rev 19, 29–38. [PubMed: 24846773]

[4]. Hatfield CF, Herbert J, van Someren EJ, Hodges JR, Hastings MH (2004) Disrupted daily activity/rest cycles in relation to daily cortisol rhythms of home-dwelling patients with early Alzheimer's dementia. Brain 127, 1061–1074. [PubMed: 14998915]

[5]. Hahn EA, Wang HX, Andel R, Fratiglioni L (2014) A change in sleep pattern may predict Alzheimer disease. Am J Geriatr Psychiatry 22, 1262–1271. [PubMed: 23954041]

[6]. DeCoursey PJ, Buggy J (1989) Circadian rhythmicity after neural transplant to hamster third ventricle: Specificity of suprachiasmatic nuclei. Brain Res 500, 263–275. [PubMed: 2605495]

[7]. Abrahamson EE, Moore RY (2001) Suprachiasmatic nucleus in the mouse: Retinal innervation, intrinsic organization and efferent projections. Brain Res 916, 172–191. [PubMed: 11597605]

[8]. Aton SJ, Colwell CS, Harmar AJ, Waschek J, Herzog ED (2005) Vasoactive intestinal polypeptide mediates circadian rhythmicity and synchrony in mammalian clock neurons. Nat Neurosci 8, 476–483. [PubMed: 15750589]

[9]. Maywood ES, Reddy AB, Wong GK, O'Neill JS, O'Brien JA, McMahon DG, Harmar AJ, Okamura H, Hastings MH (2006) Synchronization and maintenance of timekeeping in suprachiasmatic circadian clock cells by neuropeptidergic signaling. Curr Biol 16, 599–605. [PubMed: 16546085]

[10]. Yamaguchi S, Isejima H, Matsuo T, Okura R, Yagita K, Kobayashi M, Okamura H (2003) Synchronization of cellular clocks in the suprachiasmatic nucleus. Science 302, 1408–1412. [PubMed: 14631044]

[11]. Harmar AJ, Marston HM, Shen S, Spratt C, West KM, Sheward WJ, Morrison CF, Dorin JR, Piggins HD, Reubi JC, Kelly JS, Maywood ES, Hastings MH (2002) The VPAC(2) receptor is essential for circadian function in the mouse suprachiasmatic nuclei. Cell 109, 497–508. [PubMed: 12086606]

[12]. Mieda M (2019) The network mechanism of the central circadian pacemaker of the SCN: Do AVP neurons play a more critical role than expected? Front Neurosci 13, 139. [PubMed: 30858797]

[13]. Stephan FK, Zucker I (1972) Circadian rhythms in drinking behavior and locomotor activity of rats are eliminated by hypothalamic lesions. Proc Natl Acad Sci U S A 69, 1583–1586. [PubMed: 4556464]

[14]. Sawaki Y, Nihonmatsu I, Kawamura H (1984) Transplantation of the neonatal suprachiasmatic nuclei into rats with complete bilateral suprachiasmatic lesions. Neurosci Res 1, 67–72. [PubMed: 6536887]

[15]. Golombek DA, Rosenstein RE (2010) Physiology of circadian entrainment. Physiol Rev 90, 1063–1102. [PubMed: 20664079]

[16]. Stopa EG, Volicer L, Kuo-Leblanc V, Harper D, Lathi D, Tate B, Satlin A (1999) Pathologic evaluation of the human suprachiasmatic nucleus in severe dementia. J Neuropathol Exp Neurol 58, 29–39. [PubMed: 10068311]

[17]. Liu RY, Zhou JN, Hoogendijk WJ, van Heerikhuize J, Kamphorst W, Unmehopa UA, Hofman MA, Swaab DF (2000) Decreased vasopressin gene expression in the biological clock of Alzheimer disease patients with and without depression. J Neuropathol Exp Neurol 59, 314–322. [PubMed: 10759187]

[18]. Zhou JN, Hofman MA, Swaab DF (1995) VIP neurons in the human SCN in relation to sex, age, and Alzheimer's disease. Neurobiol Aging 16, 571–576. [PubMed: 8544907]

[19]. Kang JE, Lim MM, Bateman RJ, Lee JJ, Smyth LP, Cirrito JR, Fujiki N, Nishino S, Holtzman DM (2009) Amyloid-beta dynamics are regulated by orexin and the sleep-wake cycle. Science 326, 1005–1007. [PubMed: 19779148]

[20]. Roh JH, Huang Y, Bero AW, Kasten T, Stewart FR, Bateman RJ, Holtzman DM (2012) Disruption of the sleep-wake cycle and diurnal fluctuation of beta-amyloid in mice with Alzheimer's disease pathology. Sci Transl Med 4, 150ra122.

[21]. Xie L, Kang H, Xu Q, Chen MJ, Liao Y, Thiyagarajan M, O'Donnell J, Christensen DJ, Nicholson C, Iliff JJ, Takano T, Deane R, Nedergaard M (2013) Sleep drives metabolite clearance from the adult brain. Science 342, 373–377. [PubMed: 24136970]

[22]. Musiek ES, Lim MM, Yang G, Bauer AQ, Qi L, Lee Y, Roh JH, Ortiz-Gonzalez X, Dearborn JT, Culver JP, Herzog ED, Hogenesch JB, Wozniak DF, Dikranian K, Giasson BI, Weaver DR, Holtzman DM, Fitzgerald GA (2013) Circadian clock proteins regulate neuronal redox homeostasis and neurodegeneration. J Clin Invest 123, 5389–5400. [PubMed: 24270424]

[23]. Yan P, Bero AW, Cirrito JR, Xiao Q, Hu X, Wang Y, Gonzales E, Holtzman DM, Lee JM (2009) Characterizing the appearance and growth of amyloid plaques in APP/PS1 mice. J Neurosci 29, 10706–10714. [PubMed: 19710322]

[24]. Lee JE, Han PL (2013) An update of animal models of Alzheimer disease with a reevaluation of plaque depositions. Exp Neurobiol 22, 84–95. [PubMed: 23833557]

[25]. Masuda A, Kobayashi Y, Kogo N, Saito T, Saido TC, Itohara S (2016) Cognitive deficits in single App knock-in mouse models. Neurobiol Learn Mem 135, 73–82. [PubMed: 27377630]

[26]. Hall AM, Roberson ED (2012) Mouse models of Alzheimer's disease. Brain Res Bull 88, 3–12. [PubMed: 22142973]

[27]. Rogers J, Churilov L, Hannan AJ, Renoir T (2017) Search strategy selection in the Morris water maze indicates allocentric map formation during learning that underpins spatial memory formation. Neurobiol Learn Mem 139, 37–49. [PubMed: 27988312]

[28]. Gomez G, Beason-Held LL, Bilgel M, An Y, Wong DF, Studenski S, Ferrucci L, Resnick SM (2018) Metabolic syndrome and amyloid accumulation in the aging brain. J Alzheimers Dis 65, 629–639. [PubMed: 30103324]

[29]. Karakelides H, Irving BA, Short KR, O'Brien P, Nair KS (2010) Age, obesity, and sex effects on insulin sensitivity and skeletal muscle mitochondrial function. Diabetes 59, 89–97. [PubMed: 19833885]

[30]. Janson J, Laedtke T, Parisi JE, O'Brien P, Petersen RC, Butler PC (2004) Increased risk of type 2 diabetes in Alzheimer disease. Diabetes 53, 474–481. [PubMed: 14747300]

[31]. Hascup ER, Broderick SO, Russell MK, Fang Y, Bartke A, Boger HA, Hascup KN (2019) Diet-induced insulin resistance elevates hippocampal glutamate as well as VGLUT1 and GFAP expression in AbetaPP/PS1 mice. J Neurochem 148, 219–237. [PubMed: 30472734]

[32]. Ordonez-Gutierrez L, Fernandez-Perez I, Herrera JL, Anton M, Benito-Cuesta I, Wandosell F (2016) AbetaPP/PS1 transgenic mice show sex differences in the cerebellum associated with aging. J Alzheimers Dis 54, 645–656. [PubMed: 27567877]

[33]. Hascup KN, Findley CA, Sime LN, Hascup ER (2020) Hippocampal alterations in glutamatergic signaling during amyloid progression in AbetaPP/PS1 mice. Sci Rep 10, 14503. [PubMed: 32879385]

[34]. Schonheit B, Zarski R, Ohm TG (2004) Spatial and temporal relationships between plaques and tangles in Alzheimer-pathology. Neurobiol Aging 25, 697–711. [PubMed: 15165691]

[35]. Zhao J, O'Connor T, Vassar R (2011) The contribution of activated astrocytes to Abeta production: Implications for Alzheimer's disease pathogenesis. J Neuroinflammation 8, 150. [PubMed: 22047170]

[36]. Abdul HM, Sama MA, Furman JL, Mathis DM, Beckett TL, Weidner AM, Patel ES, Baig I, Murphy MP, LeVine H 3rd, Kraner SD, Norris CM (2009) Cognitive decline in Alzheimer's disease is associated with selective changes in calcineurin/NFAT signaling. J Neurosci 29, 12957–12969. [PubMed: 19828810]

[37]. Hascup KN, Findley CA, Britz J, Esperant-Hilaire N, Broderick SO, Delfino K, Tischkau S, Bartke A, Hascup ER (2021) Riluzole attenuates glutamatergic tone and cognitive decline in AbetaPP/PS1 mice. J Neurochem 156, 513–523. [PubMed: 33107040]

[38]. Thal DR, Schultz C, Dehghani F, Yamaguchi H, Braak H, Braak E (2000) Amyloid beta-protein (Abeta)-containing astrocytes are located preferentially near N-terminal-truncated Abeta deposits in the human entorhinal cortex. Acta Neuropathol 100, 608–617. [PubMed: 11078212]

[39]. Perez-Nievas BG, Serrano-Pozo A (2018) Deciphering the astrocyte reaction in Alzheimer's disease. Front Aging Neurosci 10, 114. [PubMed: 29922147]

[40]. Katsouri L, Birch AM, Renziehausen AWJ, Zach C, Aman Y, Steeds H, Bonsu A, Palmer EOC, Mirzaei N, Ries M, Sastre M (2020) Ablation of reactive astrocytes exacerbates disease pathology in a model of Alzheimer's disease. Glia 68, 1017–1030. [PubMed: 31799735]

[41]. Tso CF, Simon T, Greenlaw AC, Puri T, Mieda M, Herzog ED (2017) Astrocytes regulate daily rhythms in the suprachiasmatic nucleus and behavior. Curr Biol 27, 1055–1061. [PubMed: 28343966]

[42]. Lananna BV, McKee CA, King MW, Del-Aguila JL, Dimitry JM, Farias FHG, Nadarajah CJ, Xiong DD, Guo C, Cammack AJ, Elias JA, Zhang J, Cruchaga C, Musiek ES (2020) Chi3l1/YKL-40 is controlled by the astrocyte circadian clock and regulates neuroinflammation and Alzheimer's disease pathogenesis. Sci Transl Med 12, eaax3519. [PubMed: 33328329]

[43]. McCauley JP, Petroccione MA, D'Brant LY, Todd GC, Affinnih N, Wisnoski JJ, Zahid S, Shree S, Sousa AA, De Guzman RM, Migliore R, Brazhe A, Leapman RD, Khmaladze A, Semyanov A, Zuloaga DG, Migliore M, Scimemi A (2020) Circadian modulation of neurons and astrocytes controls synaptic plasticity in hippocampal area CA1. Cell Rep 33, 108255. [PubMed: 33053337]

[44]. Nakamura TJ, Takasu NN, Nakamura W (2016) The suprachiasmatic nucleus: Age-related decline in biological rhythms. J Physiol Sci 66, 367–374. [PubMed: 26915078]

[45]. Tahara Y, Takatsu Y, Shiraishi T, Kikuchi Y, Yamazaki M, Motohashi H, Muto A, Sasaki H, Haraguchi A, Kuriki D, Nakamura TJ, Shibata S (2017) Age-related circadian disorganization caused by sympathetic dysfunction in peripheral clock regulation. NPJ Aging Mech Dis 3, 16030. [PubMed: 28721279]

[46]. Farajnia S, Deboer T, Rohling JH, Meijer JH, Michel S (2014) Aging of the suprachiasmatic clock. Neuroscientist 20, 44–55. [PubMed: 23924666]

[47]. Jones JR, Simon T, Lones L, Herzog ED (2018) SCN VIP neurons are essential for normal light-mediated resetting of the circadian system. J Neurosci 38, 7986–7995. [PubMed: 30082421]

[48]. Mazuski C, Abel JH, Chen SP, Hermanstyne TO, Jones JR, Simon T, Doyle FJ 3rd, Herzog ED (2018) Entrainment of circadian rhythms depends on firing rates and neuropeptide release of VIP SCN neurons. Neuron 99, 555–563 e555. [PubMed: 30017392]

[49]. Sterniczuk R, Antle MC, Laferla FM, Dyck RH (2010) Characterization of the 3xTg-AD mouse model of Alzheimer's disease: Part 2. Behavioral and cognitive changes. Brain Res 1348, 149–155. [PubMed: 20558146]

[50]. Ma Z, Jiang W, Zhang EE (2016) Orexin signaling regulates both the hippocampal clock and the circadian oscillation of Alzheimer's disease-risk genes. Sci Rep 6, 36035. [PubMed: 27796320]

[51]. Volianskis A, Kostner R, Molgaard M, Hass S, Jensen MS (2010) Episodic memory deficits are not related to altered glutamatergic synaptic transmission and plasticity in the CA1 hippocampus of the APPswe/PS1deltaE9-deleted transgenic mice model of ss-amyloidosis. Neurobiol Aging 31, 1173–1187. [PubMed: 18790549]

[52]. Diaz Brinton R (2012) Minireview: Translational animal models of human menopause: Challenges and emerging opportunities. Endocrinology 153, 3571–3578. [PubMed: 22778227]

[53]. Mauvais-Jarvis F (2018) Gender differences in glucose homeostasis and diabetes. Physiol Behav 187, 20–23. [PubMed: 28843891]

[54]. Sharma G, Mauvais-Jarvis F, Prossnitz ER (2018) Roles of G protein-coupled estrogen receptor GPER in metabolic regulation. J Steroid Biochem Mol Biol 176, 31–37. [PubMed: 28223150]

[55]. Hoyer S (2002) The brain insulin signal transduction system and sporadic (type II) Alzheimer disease: An update. J Neural Transm (Vienna) 109, 341–360. [PubMed: 11956956]

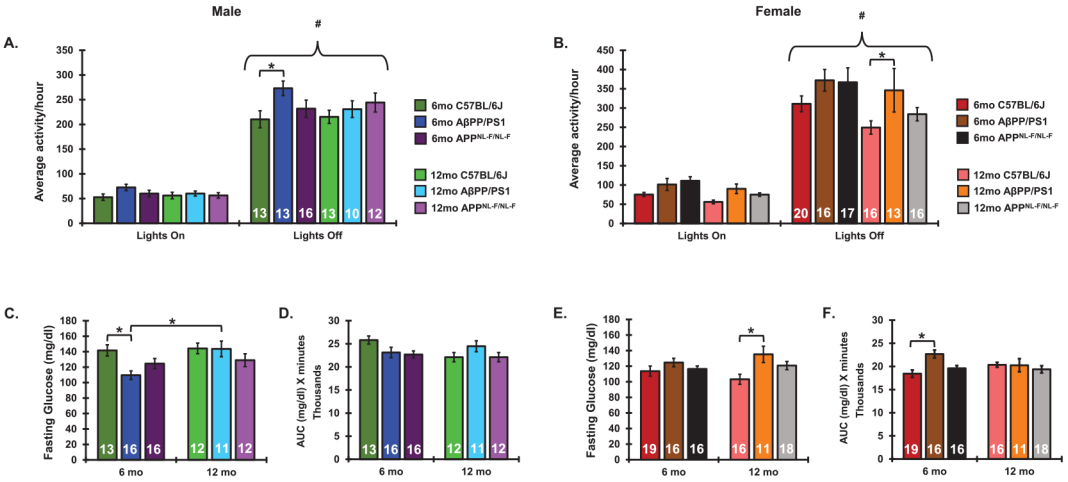

Fig. 1.

Diurnal activity patterns and glucose metabolism in aging and AD. Diurnal locomotor activity measurements in 6- and 12-month-old male (A) and female (B) C57BL/6J, AβPP/PS1, and $APP^{NL\text{-}F/NL\text{-}F}$ mice as measured via breakage of a cage-mounted infrared beam. Fasting glucose following a 15-h fast in 6- and 12-month-old male (C) and female (E) C57BL/6J, AβPP/PS1, and $APP^{NL\text{-}F/NL\text{-}F}$ mice. Glucose tolerance as measured via area under the curve of blood glucose across 120 min following a bolus of 20% glucose administered ip. in male (D) and female (F) C57BL/6J, AβPP/PS1, and $APP^{NL\text{-}F/NL\text{-}F}$ mice. Sample sizes are noted in each respective figure. *p <0.05. #p < 0.05 with respect to lights off activity within a group.

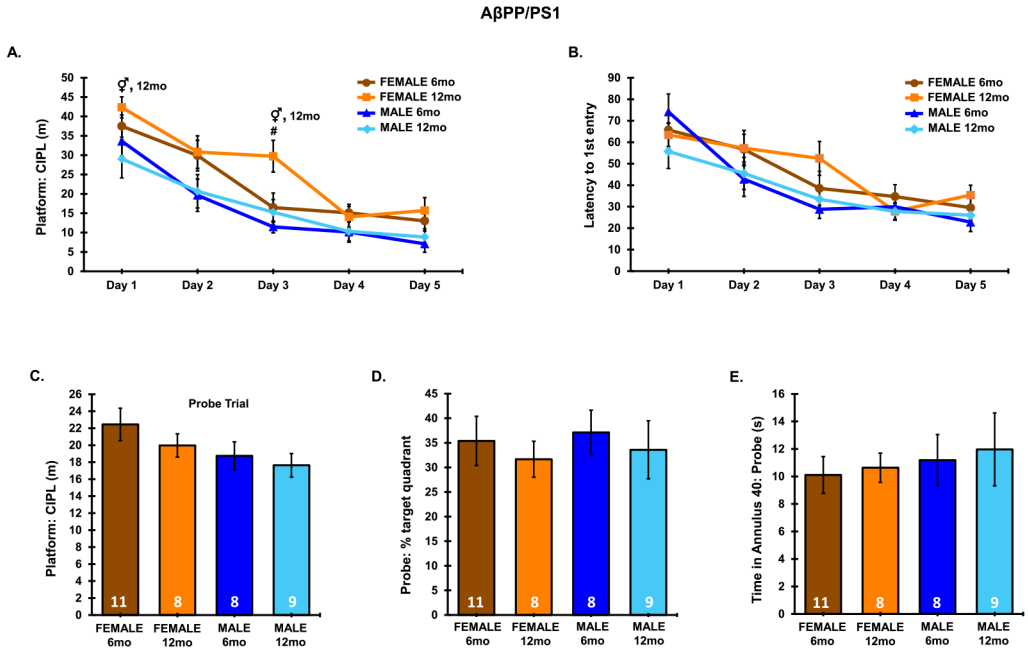

Fig. 2.

MWM training and probe challenge in AβPP/PS1 mice. Data from each of the 3 trials were averaged for each respective day of the 5-day training period. Probe data consists of a single 60-s trial. A) Platform: CIPL during the 5-day training period. B) Latency to 1st entry to the platform during the 5-day training period. C) Platform: CIPL during the probe trial. D) Percent time spent in the target quadrant during the probe trial. E) Total time spent in the annulus 40 during the probe trial. Sample Sizes for MWM are noted in the probe trial. ♀ $p < 0.05$ between sexes at the indicated age. # $p < 0.05$ between age groups within a sex.

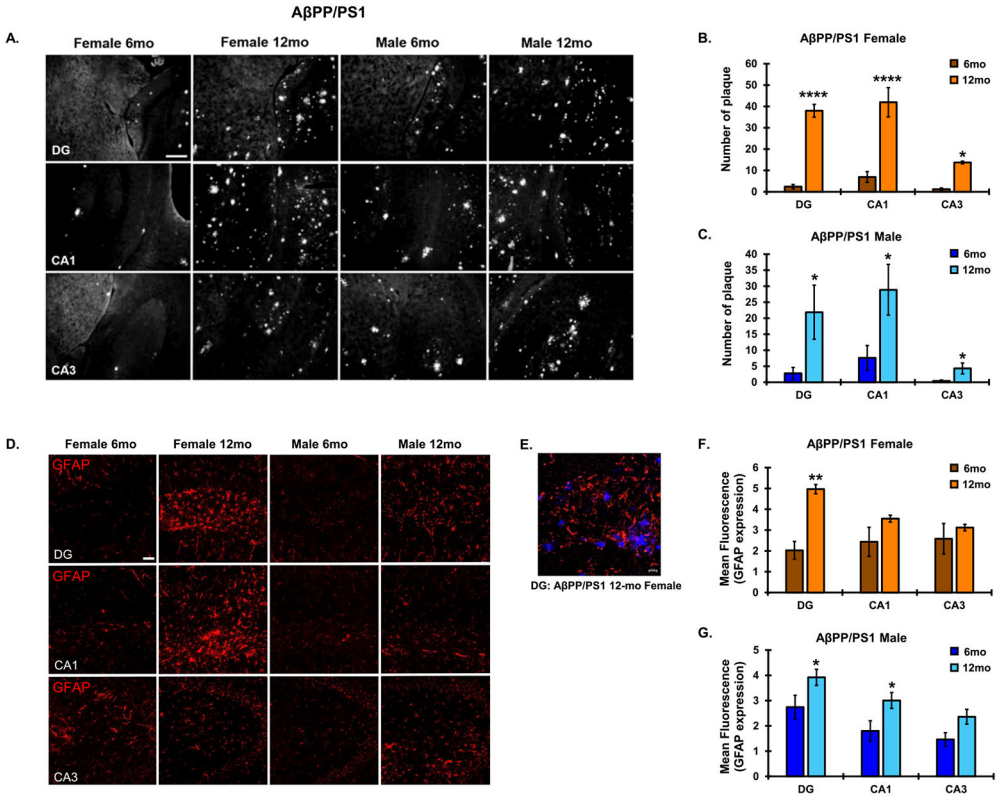

Fig. 3.

Plaque pathology and astrogliotic response in the AβPP/PS1 AD model. A) Representative plaque progression in the DG, CA1, and CA3 hippocampal subregions in male and female AβPP/PS1 animals from 6–12 months (10x magnification, scale bar = 100 μm). Average plaque number was quantitated for (B) females and (C) males across hippocampal subregions. D) Hippocampal astrocyte reactivity via GFAP IF (10x magnification, scale bar 50 μm). E) Representative astrogliotic response to amyloid plaques in a 12-month-old female AβPP/PS1 mouse (20x magnification, scale bar = 20 μm). Average mean fluorescence for GFAP IF was quantitated across hippocampal subregions in (F) female and (G) male AβPP/PS1 mice. $N = 3–4$ for all groups. *$p < 0.05$, **$p < 0.01$, ****$p < 0.0001$.

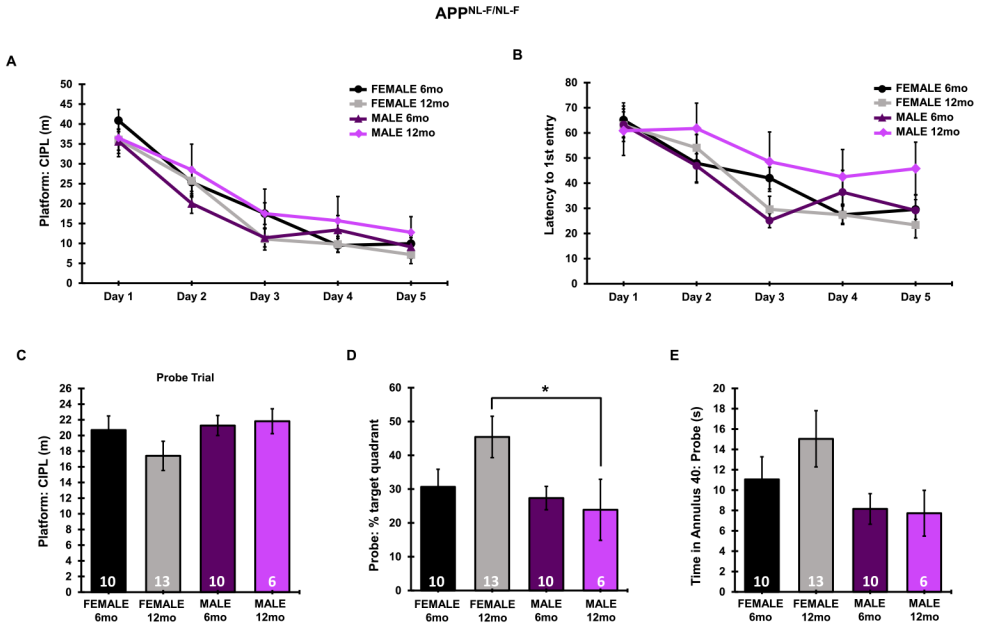

Fig. 4.

MWM training and probe challenge in APP$^{NL-F/NL-F}$ mice. A) Data from each of the 3 trials were averaged for each respective day of the 5-day training period. Probe data consists of a single 60-s trial. A) CIPL during the 5-day training period. B) Latency to 1st entry to the platform during the 5-day training period. C) Platform: CIPL during the probe trial. D) Percent time spent in the target quadrant during the probe trial. E) Total time spent in the annulus 40 during the probe trial. Sample Sizes for MWM are noted in the probe trial. *$p <$ 0.05.

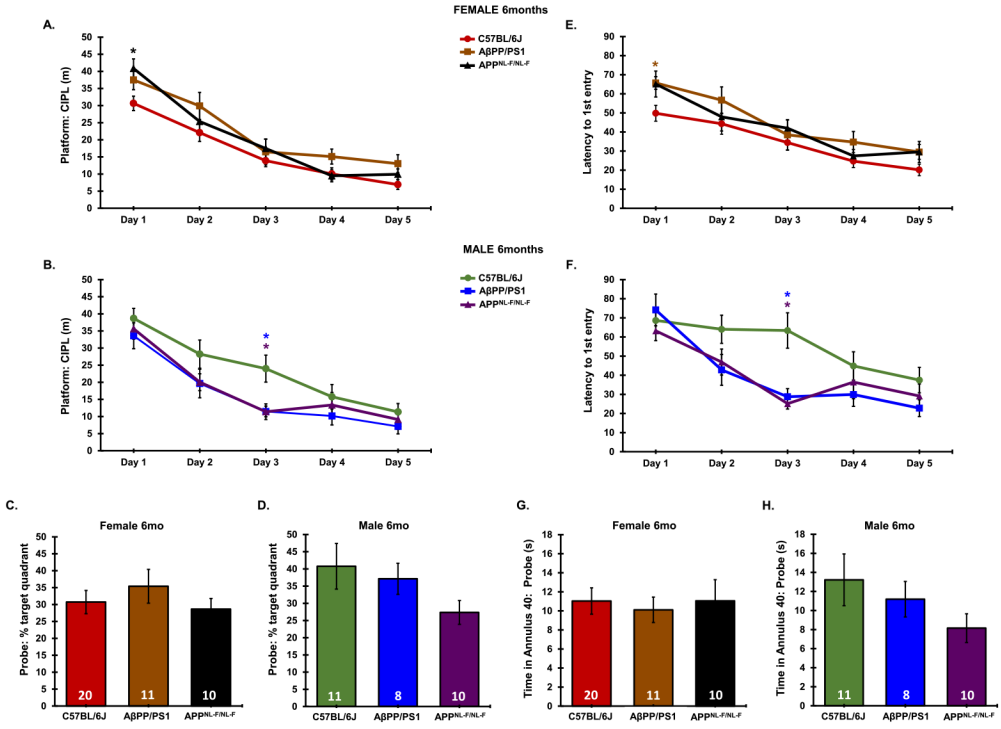

Fig. 5.

Comparative cognitive declinein 6-month-old AβPP/PS1 and $APP^{NL-F/NL-F}$ AD models. Platform: CIPL and latency to 1st platform entry was averaged across 3 independent trials per day during the 5-day training period. Probe (day 8) data was taken from a single 60-s trial. Platform: CIPL during the 5-day training period is represented in 6-month-old females (A), 6-month-old males (B). Latency to 1st platform entry is represented in 6-month-old females (E), and 6-month-old males (F). Percent time spent in the target quadrant during the probe trial is represented in 6-month-old females (C), 6-month-old males (D). Time spent in the annulus 40 during the probe trial is represented in 6-month-old females (G), and 6-month-old males (H). Sample Sizes for MWM are noted in C-H. $*p < 0.05$ with respect to C57BL/6J, color coordinated for the group being compared.

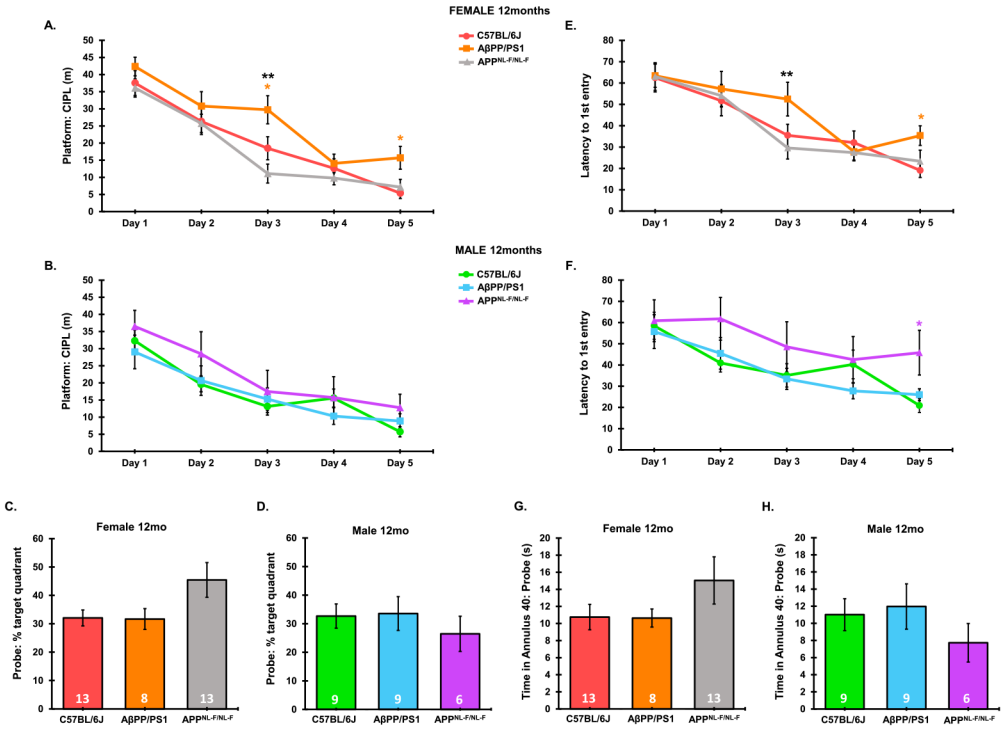

Fig. 6.

Comparative cognitive decline in 12-month AβPP/PS1 and APP$^{NL\text{-}F/NL\text{-}F}$ AD models. Platform: CIPL and latency to 1st platform entry was averaged across 3 independent trials per day during the 5-day training period. Probe (day 8) data was taken from a single 60-s trial. Platform: CIPL during the 5-day training period is represented in 12-month-old females (A), 12-month-old males (B). Latency to 1st platform entry is represented in 12-month-old females (E), and 12-month-old males (F). Percent time spent in the target quadrant during the probe trial is represented in 12-month-old females (C), 12-month-old males (D). Time spent in the annulus 40 during the probe trial is represented in 12-month-old females (G), and 12-mont-oldh males (H). Sample Sizes for MWM are noted in C-H. *$p < 0.05$ with respect to C57BL/6J, color coordinated for the group being compared. **$p < 0.05$ AβPP/PS1 versus APP$^{NL\text{-}F/NL\text{-}F}$.

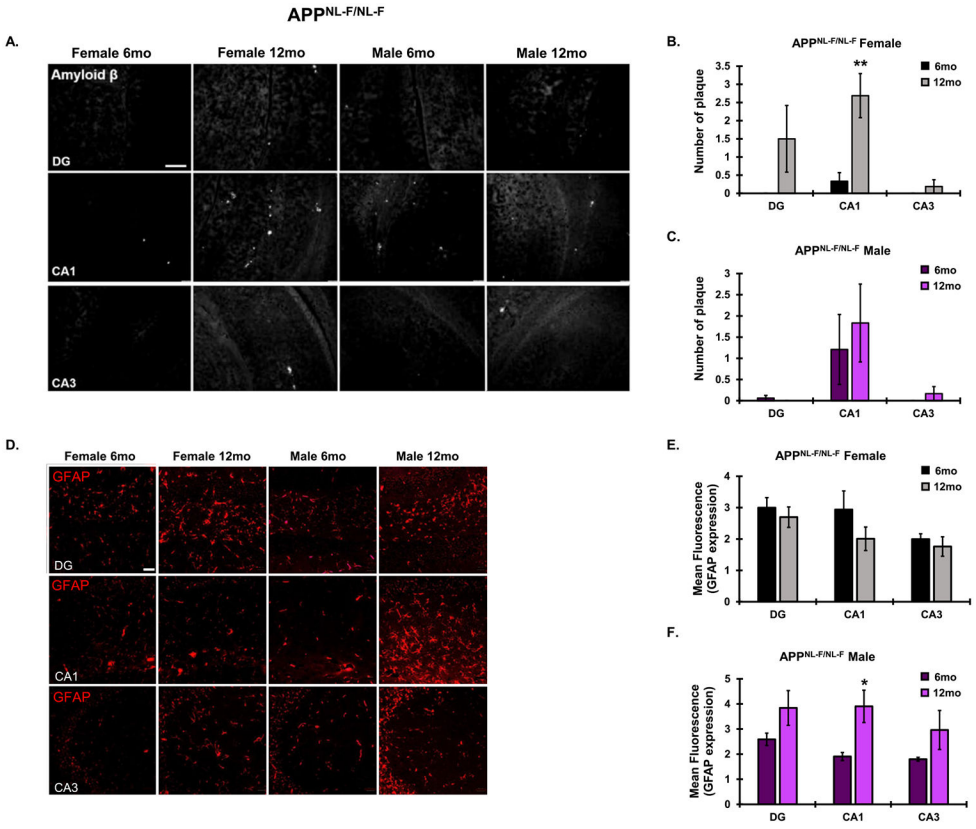

Fig. 7.

Plaque pathology and astrogliotic response in the APP$^{NL-F/NL-F}$ AD model. A) Representative plaque progression in the DG, CA1, and CA3 hippocampal subregions in male and female APP$^{NL-F/NL-F}$ animals from 6–12 months (10x magnification, scale bar = 100 μm). Average plaque number was quantitated for (B) females and (C) males across hippocampal subregions. D) Hippocampal astrocyte reactivity via GFAP IF (10x magnification, scale bar 50 μm). Average mean fluorescence for GFAP IF was quantitated across hippocampal subregions in (E) female and (F) male APP$^{NL-F/NL-F}$ mice. $N = 3–4$ for all groups. *$p < 0.05$, **$p < 0.01$.

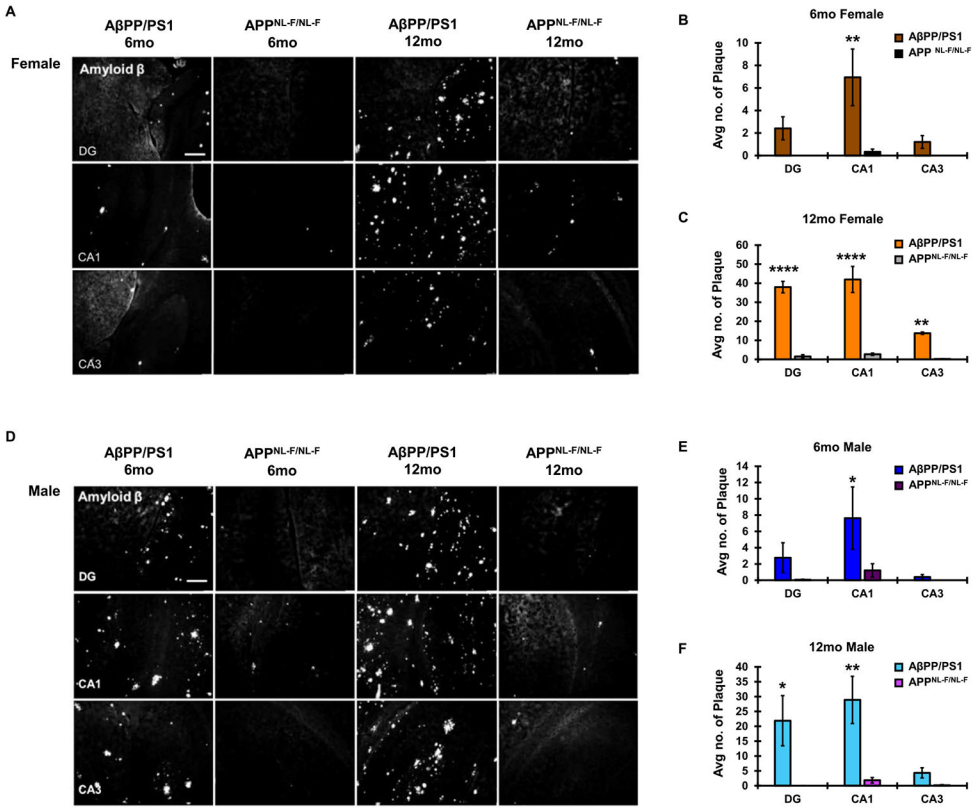

Fig. 8.

Comparative plaque pathology between AβPP/PS1 and the APP$^{NL\text{-}F/NL\text{-}F}$ AD models. A) Comparative plaque pathology in female mice at both 6- and 12-month endpoints across the DG, CA1, and CA3 hippocampal subregions (10x magnification, scale bar 100 μm). Average plaque number across hippocampal subregions was quantitated in (B) 6-month-old females and (C) 12-month-old females. D) Comparative plaque pathology in male mice at both 6- and 12-month-old endpoints across the DG, CA1, and CA3 hippocampal subregions. Average plaque number across hippocampal subregions was quantitated in (E) 6-month-old males and (F) 12-month-old males. $N = 3–4$ for all groups. *$p < 0.05$, **$p < 0.01$, ****$p < 0.0001$.

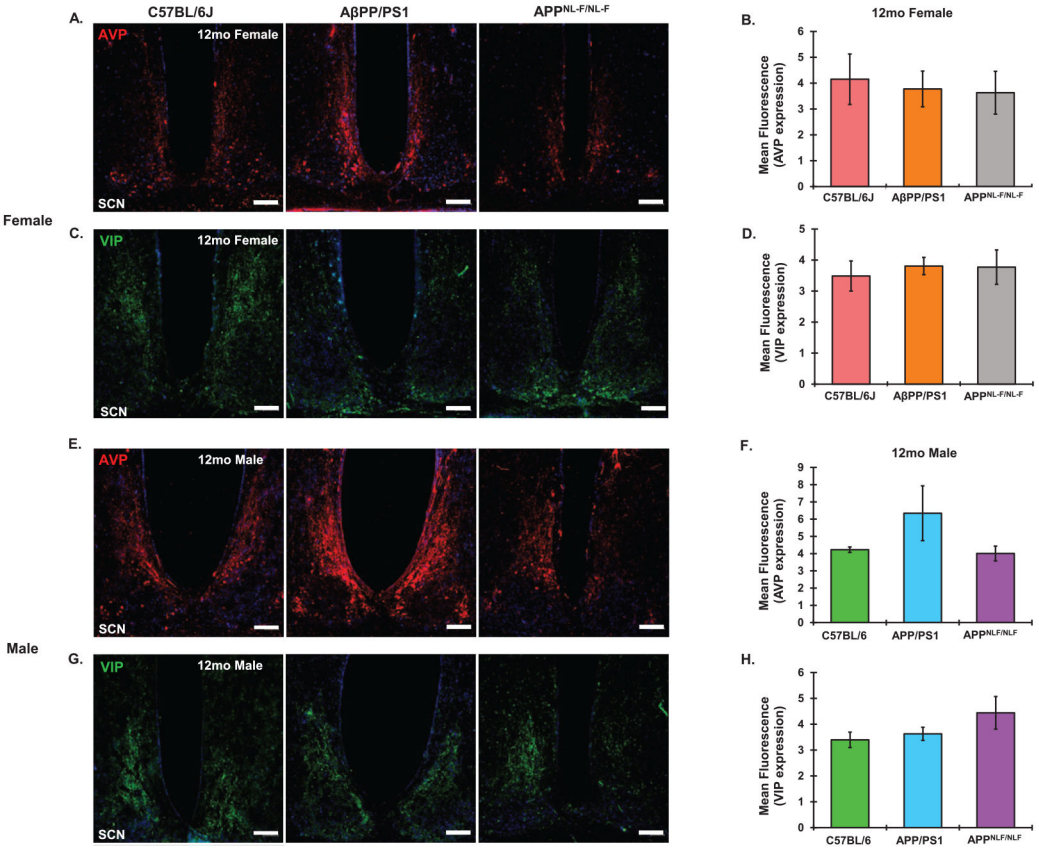

Fig. 9.

Comparative 12-month AVP and VIP expression. Representative AVP images from the SCN of 12-month-old (A) female and (E) male C57BL6J, AβPP/PS1 and APP$^{NL-F/NL-F}$ animals. Mean Fluorescent intensity of for AVP expression in (B) females and (F) males. Representative VIP images from the SCN of 12-month-old (C) female and (G)male C57BL6J, AβPP/PS1 and APP$^{NL-F/NL-F}$ animals. Mean Fluorescent intensity of for VIP expression in (D) females and (H) males. $N = 3–4$ for all groups. Scale Bar represents 100 μm. All images taken at 10x magnification.